Youngmok Jeon*

High order immersed hybridized difference methods for elliptic interface problems

https://doi.org/10.1515/jnma-2023-0011
Received January 12, 2023; revised May 07, 2023; accepted June 02, 2023

Abstract: We propose high order conforming and nonconforming immersed hybridized difference (IHD) methods in two and three dimensions for elliptic interface problems. Introducing the virtual to real transformation (VRT), we could obtain a systematic and unique way of deriving arbitrary high order methods in principle. The optimal number of collocating points for imposing interface conditions is proved, and a unique way of constructing the VRT is suggested. Numerical experiments are performed in two and three dimensions. Numerical results achieving up to the 6th order convergence in the L_2-norm are presented for the two dimensional case, and a three dimensional example with a 4th order convergence is presented.

Keywords: elliptic interface problem, hybridized difference method, immersed interface, VR transformation

Classification: 65N30, 65N38, 65N50

1 Introduction

Elliptic interface problems with a discontinuous coefficient and jump in solution appear in many engineering applications such as composite materials, fluid mechanics, biological sciences. For the last decades there has been extensive progress in developing efficient numerical schemes for these problems in the scientific computing society [14, 16, 21]. The immersed interface type methods have been one of popular choices in the fields of scientific computing and computational engineering. Some of them include the immersed boundary (IB) method [13, 20, 21], immersed interface method (IIM) [7, 14, 16], matching interface and boundary (MIB) method [25, 26], extended finite element method (XFEM) [2], immersed finite element method [1, 5, 6, 17] and kernel free boundary integral method [23, 24].

In this paper we propose a novel immersed finite difference method with theoretical justification, which we call *the immersed hybridized difference method* (IHD method). Novel ideas lie in choosing a proper number of collocation points for interface conditions and introduction of the polynomial space for nonconforming interpolation with arbitrary degrees. Those discoveries made the implementation issue of higher order methods clearer and generalize the earlier version of the IHD method in [9, 12] in which two dimensional methods up to the 4th order are presented, but three dimensional and higher order methods can not be clearly stated.

Let us consider a simple elliptic interface equation:

$$\mathcal{L}(u) = -\nabla\cdot(\varkappa\nabla u) = f \quad \text{in } \Omega \tag{1.1a}$$

$$u = 0 \quad \text{on } \partial\Omega \tag{1.1b}$$

together with the jump conditions on the interface

$$[\![u]\!]_\Gamma = w, \qquad [\![\varkappa\partial_\nu u]\!]_\Gamma = v. \tag{1.2a}$$

Here, $\Omega = \Omega^-\cup\Omega^+$, $\Gamma = \partial\Omega^-\cap\partial\Omega^+$, and the vectors $\nu^\pm$ denote the unit outward normal vectors on Γ from $\Omega^\pm$, respectively. Let $\varkappa^\pm = \varkappa|_{\Omega^\pm}$, where $\varkappa^\pm$ are given positive constants, then $[\![\varkappa\partial_\nu u]\!] = \varkappa^-\partial u^-/\partial\nu^- + \varkappa^+\partial u^+/\partial\nu^+$ and $[\![u]\!] = u^+ - u^-$ with $u^\pm = u|_{\Omega^\pm}$.

The hybridized finite difference method is composed of two different finite differences. Let us consider a decomposition of the domain into rectangular (or square) cells, $\mathcal{T}_h$ so that $\Omega = \bigcup_{R\in\mathcal{T}_h} R$. Then, the problem (1.1)

***Corresponding author: Youngmok Jeon,** Department of Mathematics, Ajou University, Suwon 16499, Korea. Email: yjeon@ajou.ac.kr

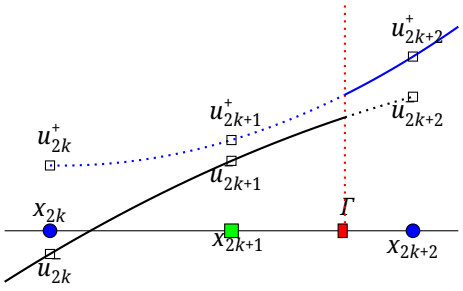

Fig. 1: One dimensional illustration of the extended solutions $u^{\pm}(x)$ in the interface cell: the solid lines represent $u^{\text{real}}(\equiv u)$ and the dotted lines represent u^{virt}.

satisfies the following localization; for $u \in C(\Omega) \cap C^2(\Omega^{\pm})$ it satisfies the *cell equation*,

$$-\nabla \cdot (\varkappa \nabla u) = f \quad \text{on } R \in \mathcal{T}_h \tag{1.3}$$

and the local solutions are patched together by the *intercell flux continuity* on cell edges,

$$[\![\varkappa \partial_\nu u]\!]_e = \varkappa \partial_\nu u|_e + \varkappa' \partial_{\nu'} u|_e = 0 \quad \text{on } e = \partial R \cap \partial R'. \tag{1.4}$$

Here, ν and ν' are the outward unit normal vectors from R and R', respectively. The finite difference approximations of equations (1.3) and (1.4) yield the hybridized difference method (HDM) [10, 22]. Let us consider a one dimensional case for a brief description of the immersed hybridized method. If u or its normal derivative $\partial_\nu u$ has discontinuity as in Fig. 1 the standard finite difference does not yield a good approximation. Therefore, we introduce the *virtual to real transformation* to accommodate jumps in solution and its flux on interface cells.

In Fig. 1 we would like to define a linear relation between $u^{\text{real}} = \{u^-_{2k}, u^-_{2k+1}, u^+_{2k+2}\}$ and $u^{\text{virt}} = \{u^+_{2k}, u^+_{2k+1}, u^-_{2k+2}\}$ so that $u^{\text{virt}} \approx \mathcal{M} u^{\text{real}} + C$. Here, $\mathcal{M}$ is a 3×3 matrix and C is a correction 3-vector. This linear relation is called the *virtual to real transformation* (VRT). The VRT will be obtained from the interface conditions and the governing differential equation, i.e.,

$$u^+(\Gamma) = u^-(\Gamma) + w, \qquad \varkappa^+ \partial_{\nu^+} u^+(\Gamma) = \varkappa^- \partial_{\nu^-} u^-(\Gamma) + v$$
$$-(\varkappa^+ u^+_x)_x(x_{2k+1}) = -(\varkappa^- u^-_x)_x(x_{2k+1}) + (f^+(x_{2k+1}) - f^-(x_{2k+1}))$$

by assuming $u^{\pm} \in \text{span}\{1, x, x^2\}$. Then, one can obtain a finite difference approximation in terms of u^{real} as follows:

$$D^h_{xx} u^-_{2k+1} = \frac{u^-_{2k+2} - 2u^-_{2k+1} + u^-_{2k}}{(h_k/2)^2} = \frac{\omega_1 u^-_{2k} + \omega_2 u^-_{2k+1} + \omega_3 u^+_{2k+2} + \widetilde{C}}{(h_k/2)^2}$$

with $h_k = x_{2k+2} - x_{2k}$ as in the immersed interface method [14–16]. The VRT is comparable with the difference equation in the correction function method (CFM) [18, 19]. The difference equation in the CFM can be obtained from the VRT here by setting $d = u^+ - u^-$ for the case $\varkappa^- = \varkappa^+$. Moreover, the VRT can be understood as a finite difference version of the Cauchy mapping in the latest papers of the IFEM [1, 5].

Our method is also comparable with the MIB (matched interface and boundary) method [25, 26].

In the immersed interface method the weight and correction $\{\omega_1, \omega_2, \omega_3, \widetilde{C}\}$ are obtained by the Taylor expansion of $u^{\pm}$ around Γ and the method of undetermined coefficients. On the process analytic differentiation of interface conditions and the governing PDE in a local coordinate system on the interface-manifold is necessary, which can be cumbersome and requires elaborated efforts to obtain a high order method in two and three dimensional cases. However, it is possible to obtain a high order method, and the compact finite difference immersed interface method achieve the 4th and 6th order convergences in the L_2-norm [3, 4]. In principle an IHD method with arbitrary order convergence is possible as well, and a 2D numerical result of the IHD method with a 6th order convergence is presented in addition to a 3D example with a 4th order convergence in Section 5.

Our approach does not need analytic handling of interface conditions and the governing PDE to obtain higher order methods in higher dimensions. In this sense our approach shares some common motivation with the MIB method. In the MIB method they introduce fictitious values, which correspond to the virtual values in the IHD. The fictitious values are solved in terms of real values by using the interface conditions, and higher

order methods can be obtained by adding fictitious values and repeating this process. On the other hand we utilize the governing PDE and interface conditions to set up the VRT.

The immersed hybridized difference method is a hybridized difference method (HDM), where the finite differences in interface cells are modified to accommodate jumps in solutions by utilizing the above mentioned VRT. There are two kinds of the hybridized difference methods, the conforming (Q_m) and nonconforming (Q_m^*) versions. Here, Q_m is the space of polynomials of degree m in each variable for either two or three dimensional spaces. In this paper we consider both the conforming and nonconforming versions of the IHD methods, however, numerical experiments are more focused on the Q_m^* method. In the HDM we need a rectangular (cubic in 3D) mesh generation of a domain as in the finite element method, and the hybridized difference is composed of two kinds of finite differences, the cell finite difference and intercell finite difference. The terms, conforming and nonconforming finite difference methods are unconventional to the computational mathematics community, but they look inevitable in our case. By the nonconforming HDM it means that the computational nodes are composed of the Gaussian points within rectangular cells and those in their faces [8]. Therefore, the reproduced polynomial solution belongs to nonconforming elements. On the other hand the conforming HDM induces a conforming solution since the computational nodes are augmented by the corner points of mesh cells [22].

The hybridized difference methods (HDM) are developed by the author and his colleagues [8, 10, 11, 22], and it is locally conservative and has an embedded static condensation property. Bearing the structure of the hybridized finite element method, the HDM derives a bilinear form which makes numerical analysis handy [8, 11]. The IHD is obtained by adopting the VRT on interface cells into the existing hybridized finite difference method.

The paper is organized as follows. In Section 2 we introduce the 1-d IHD method. This will provide some preliminary ideas on the high dimensional IHD, and we refer to the paper [9] for some elementary one dimensional stability and convergence analysis. For a high dimensional IHD the number of collocation points to impose interface conditions is non trivial. To establish high order methods in two and three dimensional problems it is essential to have knowledge on how many degrees of freedom can be consumed by interface conditions. The number of collocations of interface conditions should not be less than the nullity of the Laplace operator on $Q_m(x, y)$ and $Q_m(x, y, z)$. This issue is covered in Section 3. In here, the dimension of the harmonic polynomial space in Q_m are analyzed through two theorems and one corollary. In Section 4 higher dimensional IHD methods of the conforming (Q_m) and nonconforming (Q_m^*) versions are introduced. Since the hybridized difference method can be easily understood we will mainly discuss on construction of the VRT. For the Q_m^* method a general formula for constructing the Q_m^* polynomial space is suggested. The Q_m^* method has some advantages over the Q_m method in the sense that (1) the former has much less degrees of freedom in the VRT and global stiffness system and (2) it can manage problems with a complicated geometric shape of an interface more stably. Section 5 is devoted to numerical experiments. Two and three dimensional examples with simple and complicated geometric shapes of interface are considered. Numerical results show satisfactory convergence for two dimensional cases. For the three dimensional problem, although computation can not be performed up to a fine scale because of very high computational cost involved, we observe promising numerical results. A brief discussion is presented in the final section.

2 Review of one dimensional IHD method

We begin with introducing the lowest order IHD method in one dimensional space (it corresponds the case $m = 2$), and it will give a preliminary idea for higher dimensional problems. Consider a unit interval $[0, 1]$ with an interface point Γ and its partition into N-cells so that $[0, 1] = \bigcup_{j=0}^{N-1} I_j$ with $I_j = [x_{2j}, x_{2j+2}]$ and $\Gamma \in I_k$ for some k. The *regular* cell is meant by a non-interface cell and the *interface* cell contains an interface point Γ as in Fig. 2.

Let us consider an elliptic interface equation with the Dirichlet condition on $I = [0, 1]$:

$$-(\varkappa u_x)_x = f \quad \text{on } I \setminus \Gamma, \qquad u(0) = 0, \quad u(1) = 0 \tag{2.1}$$

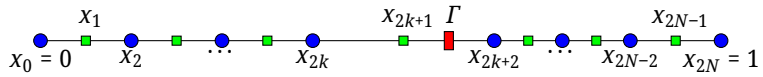

Fig. 2: One dimensional cell configuration: cell-point, interface, intercell point.

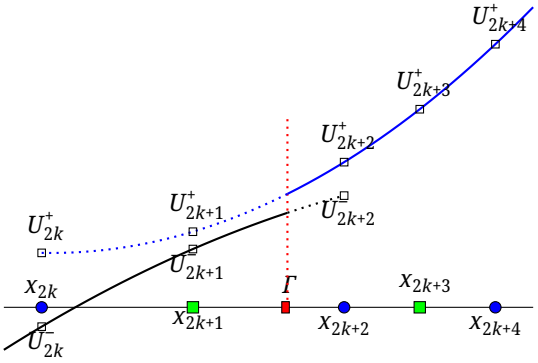

Fig. 3: An illustration of the extended solutions $U^{\pm}(x)$ in the interface cell: the solid lines represent $U^{\text{real}}(\equiv U)$ and the dotted lines represent U^{virt}.

with the jump conditions at the interface point Γ,

$$[\![u]\!]_\Gamma = u^+(\Gamma) - u^-(\Gamma) = w, \qquad [\![\varkappa \partial_\nu u]\!]_\Gamma = \varkappa^+ D_{-x} u^+(\Gamma) + \varkappa^- D_x u^-(\Gamma) = v. \tag{2.2}$$

Here, $D_{-x} = -D_x$ and

$$u(x) = \begin{cases} u^-(x), & x \in [0, \Gamma] \\ u^+(x), & x \in (\Gamma, 1]. \end{cases}$$

Our new approach is based on the virtual extension of u^- and u^+ within the interface cell $I_k = [x_{2k}, x_{2k+2}]$. The virtual extension means fictitiously extended solutions within the interface cell I_k. This approach will facilitate derivation of high order methods for interface problems as in the MIB method ([25, 26]). The interface conditions (2.2) will be contained in the process of the virtual extension (an inner process).

In the IHD method we seek the unique relation between the real solution (u^{real}) and the virtual solution (u^{virt}) via the *virtual to real (VR) transformation* on the interface cell $I_k = [x_{2k}, x_{2k+2}]$, where

$$u^{\text{real}} = \begin{cases} u^-(x), & x \in [x_{2k}, \Gamma] \\ u^+(x), & x \in [\Gamma, x_{2k+2}], \end{cases} \qquad u^{\text{virt}} = \begin{cases} u^+(x), & x \in [x_{2k}, \Gamma] \\ u^-(x), & x \in [\Gamma, x_{2k+2}]. \end{cases}$$

Note that $u = u^{\text{real}}$ on I_k. Let U be the approximate solution of u and $U^{\pm}$ those of $u^{\pm}$. We are going to have the six function values for the extended solutions as follows (see the interval I_k in Fig. 3):

$$\{U^-_{2k}, U^-_{2k+1}, U^-_{2k+2}, U^+_{2k}, U^+_{2k+1}, U^+_{2k+2}\}.$$

Among them $U^{\text{real}} = \{U^-_{2k}, U^-_{2k+1}, U^+_{2k+2}\}$ are the *real* values, and $U^{\text{virt}} = \{U^+_{2k}, U^+_{2k+1}, U^-_{2k+2}\}$ the *virtual* values. We suggest the following set of equations that relate U^{real} and U^{virt}:

$$U^+(\Gamma) = U^-(\Gamma) + w : U\text{-jump} \tag{2.3a}$$

$$\varkappa^+ U^+_{-x}(\Gamma) = -\varkappa^- U^-_x(\Gamma) + v : \text{ flux jump} \tag{2.3b}$$

$$-\varkappa^+ U^+_{xx}(x_{2k+1}) = -\varkappa^- U^-_{xx}(x_{2k+1}) + g : \text{ consistency} \tag{2.3c}$$

with $g = f^+(x_{2k+1}) - f^-(x_{2k+1})$. Note that we have $g = 0$ if f is smooth across the interface.

Let $U^- = U^-_{2k}\varphi_1 + U^-_{2k+1}\varphi_2 + U^-_{2k+2}\varphi_3$ and $U^+ = U^+_{2k}\varphi_1 + U^+_{2k+1}\varphi_2 + U^+_{2k+2}\varphi_3$, where $\{\varphi_1, \varphi_2, \varphi_3\} \subset P_2(I_k) = [1, x, x^2]$ are the Lagrange basis. From here on, $[1, x, \dots, x^n] \equiv \text{span}\{1, x, \dots, x^n\}$. It is easy to see that (2.3) can

be written in a matrix–vector form as follows:

$$\begin{bmatrix} \varphi_1(\Gamma) & \varphi_2(\Gamma) & \varphi_3(\Gamma) \\ -\varkappa^+\varphi_1'(\Gamma) & -\varkappa^+\varphi_2'(\Gamma) & -\varkappa^+\varphi_3'(\Gamma) \\ -\varkappa^+\varphi_1''(x_{2k+1}) & -\varkappa^+\varphi_2''(x_{2k+1}) & -\varkappa^+\varphi_3''(x_{2k+1}) \end{bmatrix} \begin{bmatrix} U_{2k}^+ \\ U_{2k+1}^+ \\ U_{2k+2}^+ \end{bmatrix} \tag{2.4}$$
$$= \begin{bmatrix} \varphi_1(\Gamma) & \varphi_2(\Gamma) & \varphi_3(\Gamma) \\ -\varkappa^-\varphi_1'(\Gamma) & -\varkappa^-\varphi_2'(\Gamma) & -\varkappa^-\varphi_3'(\Gamma) \\ -\varkappa^-\varphi_1''(x_{2k+1}) & -\varkappa^-\varphi_2''(x_{2k+1}) & -\varkappa^-\varphi_3''(x_{2k+1}) \end{bmatrix} \begin{bmatrix} U_{2k}^- \\ U_{2k+1}^- \\ U_{2k+2}^- \end{bmatrix} + \begin{bmatrix} w \\ v \\ g \end{bmatrix}.$$

Separating the real and virtual variables, equation (2.4) can be rewritten as

$$\begin{bmatrix} \varphi_1(\Gamma) & \varphi_2(\Gamma) & -\varphi_3(\Gamma) \\ -\varkappa^+\varphi_1'(\Gamma) & -\varkappa^+\varphi_2'(\Gamma) & \varkappa^-\varphi_3'(\Gamma) \\ -\varkappa^+\varphi_1''(x_{2k+1}) & -\varkappa^+\varphi_2''(x_{2k+1}) & \varkappa^-\varphi_3''(x_{2k+1}) \end{bmatrix} \begin{bmatrix} U_{2k}^+ \\ U_{2k+1}^+ \\ U_{2k+2}^- \end{bmatrix}$$
$$= \begin{bmatrix} \varphi_1(\Gamma) & \varphi_2(\Gamma) & -\varphi_3(\Gamma) \\ -\varkappa^-\varphi_1'(\Gamma) & -\varkappa^-\varphi_2'(\Gamma) & \varkappa^+\varphi_3'(\Gamma) \\ -\varkappa^-\varphi_1''(x_{2k+1}) & -\varkappa^-\varphi_2''(x_{2k+1}) & \varkappa^+\varphi_3''(x_{2k+1}) \end{bmatrix} \begin{bmatrix} U_{2k}^- \\ U_{2k+1}^- \\ U_{2k+2}^+ \end{bmatrix} + \begin{bmatrix} w \\ v \\ g \end{bmatrix}$$

or

$$\mathcal{A}[U_{2k}^+, U_{2k+1}^+, U_{2k+2}^-]^T = \mathcal{B}[U_{2k}^-, U_{2k+1}^-, U_{2k+2}^+]^T + [w, v, g]^T$$

in a symbolic form. Then, we can obtain the VRT such that

$$[U_{2k}^+, U_{2k+1}^+, U_{2k+2}^-]^T = \mathcal{M}[U_{2k}^-, U_{2k+1}^-, U_{2k+2}^+]^T + \mathcal{L}[w, v, g]^T \tag{2.5}$$

where $\mathcal{M} = \mathcal{A}^{-1}\mathcal{B}$ and $\mathcal{L} = \mathcal{A}^{-1}$. Even though equation (2.5) is the final form of the VRT, equations (2.3) also will be referred to under the same name.

With $\mathcal{M} = [M_{ij}]$ and $\mathcal{L} = [L_{ij}]$, $U_{2k+2}^- = M_{31}U_{2k}^- + M_{32}U_{2k+1}^- + M_{33}U_{2k+2}^+ + L_{31}w + L_{32}v + L_{33}g$. Then, the cell difference becomes

$$\begin{aligned} -\varkappa^- D_{xx}^h U_{2k+1}^- &= -\varkappa^- \frac{U_{2k}^- - 2U_{2k+1}^- + U_{2k+2}^-}{(h_k/2)^2} \\ &= -\varkappa^- \frac{\omega_1 U_{2k}^- + \omega_2 U_{2k+1}^- + \omega_3 U_{2k+2}^+ + C}{(h_k/2)^2} \end{aligned}$$

with

$$\omega_1 = 1 + M_{31}, \quad \omega_2 = -2 + M_{32}, \quad \omega_3 = M_{33}, \quad C = L_{31}w + L_{32}v + L_{33}g.$$

By a similar way, using that

$$\begin{aligned} U_{2k}^+ &= M_{11}U_{2k}^- + M_{12}U_{2k+1}^- + M_{13}U_{2k+2}^+ + L_{11}w + L_{12}v + L_{13}g \\ U_{2k+1}^+ &= M_{21}U_{2k}^- + M_{22}U_{2k+1}^- + M_{23}U_{2k+2}^+ + L_{21}w + L_{22}v + L_{23}g \end{aligned}$$

the intercell difference satisfies

$$\begin{aligned} (D_x^h + D_{-x}^h)U_{2k+2}^+ &= \frac{U_{2k}^+ - 4U_{2k+1}^+ + 3U_{2k+2}^+}{h_k} + \frac{3U_{2k+2}^+ - 4U_{2k+3}^+ + U_{2k+4}^+}{h_{k+1}} \\ &= \frac{\gamma_1 U_{2k}^- + \gamma_2 U_{2k+1}^- + \gamma_3 U_{2k+2}^+ + D}{h_k} + \frac{3U_{2k+2}^+ - 4U_{2k+3}^+ + U_{2k+4}^+}{h_{k+1}} \end{aligned}$$

where

$$\gamma_1 = M_{11} - 4M_{21}, \quad \gamma_2 = M_{12} - 4M_{22}, \quad \gamma_3 = M_{13} - 4M_{23} + 3$$

$$D = (L_{11} - 4L_{21})w + (L_{12} - 4L_{22})v + (L_{13} - 4L_{23})g.$$

The VRT will facilitate the process of obtaining high order finite differences especially for higher dimensional problems.

Once the finite differences are obtained on the interface cell and regular cells, the (immersed) hybridized difference method for PDE (2.1) with reference to the mesh Fig. 2 goes as follows. The hybridized difference is composed of two kinds of finite differences; *cell finite difference* and *intercell finite difference*. At the cell point $x = x_{2j+1}$ the cell finite difference approximates the PDE as

$$-\varkappa^- D^h_{xx} U_{2j+1} = f_{2j+1}, \quad j = 0, 1, \dots, N-1$$

and the intercell finite difference approximates flux continuity as

$$(D^h_x + D^h_{-x}) U_{2j} = 0, \quad j = 1, 2, \dots, N-1$$

with the boundary condition $U_0 = U_{2N} = 0$.

To obtain the P_m method we will consider the interface cell $I_k = [x_{mk}, x_{m(k+1)}]$ with the interior cell points $\{x_{mk+1}, x_{mk+2}, \dots, x_{mk+m-1}\}$ that are the Gauss points on I_k. Then, the VRT is obtained by solving the two interface conditions and $(m-1)$-consistency conditions as follows.

$$U^+(\Gamma) = U^-(\Gamma) + w : U\text{-jump} \tag{2.6a}$$

$$\varkappa^+ U^+_{-x}(\Gamma) = -\varkappa^- U^-_x(\Gamma) + v : \text{ flux jump} \tag{2.6b}$$

$$-\varkappa^+ U^+_{xx}(x_{mk+j}) = -\varkappa^- U^-_{xx}(x_{mk+j}) + g_j \quad (j = 1, \dots, m-1) : \text{consistency} \tag{2.6c}$$

with $g_j = f^+(x_{mk+j}) - f^-(x_{mk+j})$. Convergence and ellipticity analysis for one dimensional IHD method can be found in [9]. It is not comfortable to derive a high order method in the immersed interface method(IIM) even though there have been developed high order methods lately [3, 4]. The reason is that artificial interface conditions must be induced to get enough number of constraints, which involves tangential derivatives (along the interface for 2 or 3 dimensional problems) of the jump conditions and repeated differentiation of the governing PDE. In the VRT approach we do not need any artificial interface condition, and that will facilitate the construction of high order methods. The very similar idea was adopted to develop high order immersed finite element methods [1, 5]. The VRT with the homogeneous jump conditions corresponds to the Cauchy mapping in the IFEM and the non-homogeneous jump conditions can be treated through an enhanced shape function.

We finish this section by commenting on the generation of high order finite difference stencils.

Remark 2.1. Generation of high order finite difference stencils by using the Lagrange interpolation can be cumbersome because it needs analytic differentiation of the Lagrange basis. In our programing we use another approach that minimizes analytic manipulation.

Suppose $u(x) = \sum_{i=0}^m c_i x^m$ and let $u_j = u(\eta_j), j = 0, \dots, m$. Then, the coefficient vector $\mathbf{c} = (c_0, c_1, \dots, c_m)^T$ satisfies

$$\begin{bmatrix} 1 & \eta_0 & \cdots & \eta_0^m \\ 1 & \eta_1 & \cdots & \eta_1^m \\ \cdots & \cdots & \cdots & \cdots \\ 1 & \eta_j & \cdots & \eta_j^m \\ \cdots & \cdots & \cdots & \cdots \\ 1 & \eta_m & \cdots & \eta_m^m \end{bmatrix} \begin{bmatrix} c_0 \\ c_1 \\ \cdots \\ c_i \\ \cdots \\ c_m \end{bmatrix} = \begin{bmatrix} u_0 \\ u_1 \\ \cdots \\ u_j \\ \cdots \\ u_m \end{bmatrix}. \tag{2.7}$$

In a symbolic form let's write it as $A\mathbf{c} = \mathbf{u}$, and the followings are straightforward

$$u(x) = [1 \ x \ x^2 \ \cdots \ x^m] A^{-1}\mathbf{u}$$
$$D_x u(x) = [0 \ 1 \ 2x \ \cdots \ mx^{m-1}] A^{-1}\mathbf{u}$$
$$D_{xx} u(x) = [0 \ 0 \ 2 \ \cdots \ m(m-1)x^{m-2}] A^{-1}\mathbf{u}.$$

Therefore, the finite difference stencils are obtained as follows in a vector form:

$$[D^h_x u(x_j)]_{\text{stencil}} = [0 \ 1 \ 2x_j \ \cdots \ mx_j^m] A^{-1}, \qquad [D^h_{xx} u(x_j)]_{\text{stencil}} = [0 \ 0 \ 2 \ \cdots \ m(m-1)x_j^{m-1}] A^{-1}.$$

3 Interface conditions in higher dimensions

In this section we discuss how many collocation points are needed to implement the interface conditions in the VRT for two and three dimensional cases. To find the number of collocation points on the interface it is necessary to know the *nullity* of the Laplacian operator. Let $\mathcal{N}_m$ be the null space for the Laplacian operator $\Delta : Q_m \to Q_m$, where Q_m is the 2D or 3D polynomial spaces of degree m for each variable.

Theorem 3.1 (2D case). *Let* $\mathcal{N}_m = \{p \in Q_m(x, y) : \Delta p = 0\}$. *Then,*

$$\dim(\mathcal{N}_m) = \begin{cases} 2m+1, & m: \textit{even} \\ 2m+2, & m: \textit{odd}. \end{cases}$$

Proof. Let $u(x) = \sum_{j=0}^{m} u_j(x)y^j$ with $u_j \in P_m(x)$. Then,

$$\begin{aligned} \Delta u &= D_{xx}u_0 + D_{xx}u_1 y + \sum_{j=2}^{m}(D_{xx}u_j y^j + u_j j(j-1)y^{j-2}) \\ &= \sum_{j=0}^{m-2}(D_{xx}u_j + (j+2)(j+1)u_{j+2})y^j + D_{xx}u_{m-1}y^{m-1} + D_{xx}u_m y^m = 0. \end{aligned}$$

This yields a system of differential equations:

$$D_{xx}u_m = 0, \qquad D_{xx}u_{m-1} = 0 \tag{3.1a}$$
$$D_{xx}u_{m-2} + m(m-1)u_m = 0, \qquad D_{xx}u_{m-3} + (m-1)(m-2)u_{m-1} = 0 \tag{3.1b}$$
$$\cdots$$
$$D_{xx}u_1 + 6u_3 = 0, \qquad D_{xx}u_0 + 2u_2 = 0 \tag{3.1c}$$

for $m = 2k+1$, and

$$D_{xx}u_m = 0, \qquad D_{xx}u_{m-1} = 0 \tag{3.2a}$$
$$D_{xx}u_{m-2} + m(m-1)u_m = 0, \qquad D_{xx}u_{m-3} + (m-1)(m-2)u_{m-1} = 0 \tag{3.2b}$$
$$\cdots$$
$$D_{xx}u_2 + 12u_4 = 0, \qquad D_{xx}u_1 + 6u_3 = 0,$$
$$D_{xx}u_0 + 2u_2 = 0 \tag{3.2c}$$

for $m = 2k$.

When $m = 2k+1$, equations (3.1) imply

$$D_{xx}u_m = 0, \qquad D_{xx}u_{m-1} = 0 \tag{3.3a}$$
$$D_{xx}^2 u_{m-2} = 0, \qquad D_{xx}^2 u_{m-3} = 0 \tag{3.3b}$$
$$\cdots$$
$$D_{xx}^{k+1}u_1 = 0, \qquad D_{xx}^{k+1}u_0 = 0. \tag{3.3c}$$

Remember the notation, $[1, x, \ldots, x^j] = \text{span}\{1, x, \ldots, x^j\}$. The left column of equations (3.3) can be solved as

$$u_m \in [1, x], \quad u_{m-2} \in [1, x, x^2, x^3], \quad \ldots, \quad u_1 \in [1, x, \ldots, x^m].$$

Once, u_1 is known, then $\{u_3, \ldots, u_m\}$ are determined sequentially by (3.1). By the same way, the right column of equations (3.3) can be solved as

$$u_{m-1} \in [1, x], \quad u_{m-3} \in [1, x, x^2, x^3], \quad \ldots, \quad u_0 \in [1, x, \ldots, x^m].$$

The solution u_0 determines $\{u_2, u_4, \ldots, u_{m-1}\}$ sequentially. Therefore, the dimension of harmonic polynomials in $Q_m(x, y)$ is $2m+2$.

For $m = 2k$ by a similar way,

$$D_{xx}u_m = 0, \qquad D_{xx}u_{m-1} = 0 \tag{3.4a}$$
$$D_{xx}^2 u_{m-2} = 0, \qquad D_{xx}^2 u_{m-3} = 0 \tag{3.4b}$$
$$\cdots$$
$$D_{xx}^k u_2 = 0, \qquad D_{xx}^k u_1 = 0 \tag{3.4c}$$
$$D_{xx}^{k+1} u_0 = 0. \tag{3.4d}$$

Let us look at the left column of equations (3.4), we should take $u_m \in [1]$ instead of $u_m \in [1, x]$. If $u_m \in [1, x]$, $u_0 \in [1, x, \dots x^{m+1}]$ and we will have $u \notin Q_m(x, y)$. Therefore,

$$u_m \in [1], \quad u_{m-2} \in [1, x, x^2], \quad \dots, \quad u_0 \in [1, x, \dots, x^m].$$

For the right column we have

$$u_{m-1} \in [1, x], \quad u_{m-3} \in [1, x, x^2, x^3], \quad \dots, \quad u_1 \in [1, x, \dots, x^{m-1}].$$

Then, the dimension of harmonic polynomials in $Q_m(x, y)$ is $2m + 1$. □

Now, we proceed to the 3D case. It is important to note that the dimension of harmonic polynomials in $Q_m(x, y)$ is $2 \times \text{nullity}(D_{xx}^{k+1})$ for $m = 2k + 1$ and $\text{nullity}(D_{xx}^{k+1}) + \text{nullity}(D_{xx}^k)$ for $m = 2k$, where the null is taken in $P_m(x)$.

Let us introduce the space of the k-harmonic binomials:

$$\mathcal{M}_{m,k} = \{p \in Q_m(x, y) : \Delta^k p = 0\}.$$

Theorem 3.2. *For* $\mathcal{N}_m = \{p \in Q_m(x, y, z) : \Delta p = 0\}$,

$$\dim(\mathcal{N}_m) = \begin{cases} 2\dim(\mathcal{M}_{m,k+1}), & m = 2k + 1 \\ \dim(\mathcal{M}_{m,k+1}) + \dim(\mathcal{M}_{m,k}), & m = 2k. \end{cases}$$

Proof. Let $u(x, y, z) = \sum_{j=0}^m u_j(x, y)z^j \in Q_m(x, y, z)$ with $u_j \in Q_m(x, y)$. Then, $u \in \mathcal{N}_m$ implies

$$\Delta u = \sum_{j=0}^{m-2} (\Delta_z u_j + (j + 2)(j + 1)u_{j+2})z^j + \Delta_z u_{m-1} z^{m-1} + \Delta_z u_m z^m = 0$$

where $\Delta_z u = u_{xx} + u_{yy}$. As in the two dimensional case this yields that

$$\Delta_z u_m = 0, \qquad \Delta_z u_{m-1} = 0 \tag{3.5a}$$
$$\Delta_z u_{m-2} + m(m-1)u_m = 0, \qquad \Delta_z u_{m-3} + (m-1)(m-2)u_{m-1} = 0 \tag{3.5b}$$
$$\cdots$$
$$\Delta_z u_1 + 6u_3 = 0, \qquad \Delta_z u_0 + 2u_2 = 0 \tag{3.5c}$$

for $m = 2k + 1$, and

$$\Delta_z u_m = 0, \qquad \Delta_z u_{m-1} = 0 \tag{3.6a}$$
$$\Delta_z u_{m-2} + m(m-1)u_m = 0, \qquad \Delta_z u_{m-3} + (m-1)(m-2)u_{m-1} = 0 \tag{3.6b}$$
$$\cdots$$
$$\Delta_z u_2 + 12u_4 = 0, \qquad \Delta_z u_1 + 6u_3 = 0$$
$$\Delta_z u_0 + 2u_2 = 0 \tag{3.6c}$$

for $m = 2k$. When $m = 2k + 1$, equations (3.5) satisfy

$$\Delta_z u_m = 0, \qquad \Delta_z u_{m-1} = 0$$
$$\Delta_z^2 u_{m-2} = 0, \qquad \Delta_z^2 u_{m-3} = 0$$
$$\cdots$$
$$\Delta_z^{k+1} u_1 = 0, \qquad \Delta_z^{k+1} u_0 = 0.$$

When $m = 2k$, equations (3.6) satisfy

$$\begin{aligned} \Delta_z u_m = 0, \quad & \Delta_z u_{m-1} = 0 \\ \Delta_z^2 u_{m-2} = 0, \quad & \Delta_z^2 u_{m-3} = 0 \\ & \cdots \\ \Delta_z^k u_2 = 0, \quad & \Delta_z^k u_1 = 0 \\ \Delta_z^{k+1} u_0 = 0. & \end{aligned}$$

Then, the theorem is immediate. □

Corollary 3.1. For $Q_m(x, y, z)$,

$$\dim(\mathcal{N}_m) = \begin{cases} 13, & m = 2 \\ 24, & m = 3 \\ 37, & m = 4. \end{cases}$$

Proof. For $Q_2(x, y) = [1, x, y, x^2, xy, y^2, x^2y, xy^2, x^2y^2]$,

$$\Delta Q_2(x, y) = [1, x, y, (x^2 + y^2)], \qquad \Delta^2 Q_2(x, y) = [1].$$

Then, $\dim(\mathcal{M}_{2,1}) = 5$ and $\dim(\mathcal{M}_{2,2}) = 8$. Hence, $\dim(\mathcal{N}_2) = 13$.

For $Q_3(x, y) = [1, x, y, x^2, xy, y^2, x^3, x^2y, xy^2, y^3, x^3y, x^2y^2, xy^3, x^3y^2, x^2y^3, x^3y^3]$,

$$\Delta^2 Q_3(x, y) = [1, x, y, xy].$$

Therefore, $\dim(\mathcal{M}_{3,2}) = 12$. Hence, $\dim(\mathcal{N}_3) = 24$.

For $Q_4(x, y)$ we have

$$\Delta^2(Q_4(x, y)) = [1, x, y, xy, x^2, y^2, x^3 + 6xy^2, 6x^2y + y^3, x^4 + 12x^2y^2 + y^4], \qquad \Delta^3(Q_4(x, y)) = [1, x, y, x^2 + y^2].$$

Then, $\dim(\mathcal{M}_{4,2}) = 16$ and $\dim(\mathcal{M}_{4,3}) = 21$. Therefore, $\dim(\mathcal{N}_4) = 37$. □

Theorems 3.1 and 3.2 tell us how many interface conditions are needed to define a VR-transformation uniquely, that is, #(interface conditions) = $\dim(\mathcal{N}_m)$. Then, we impose the interface conditions as follows

$$\begin{cases} (J + 1)\ U\text{-jump} \oplus J\ \text{flux-jump} & \text{when } \dim(\mathcal{N}_m) = 2J + 1 \\ (J + 1)\ U\text{-jump} \oplus (J + 1)\ \text{flux-jump} & \text{when } \dim(\mathcal{N}_m) = 2J + 2. \end{cases}$$

It is very natural to choose $(J+1)$-collocation points on the interface to impose the interface conditions for either case.

4 IHD methods in higher dimension

With the help of Theorems in §3 we extend one dimensional schemes to higher dimensional ones. Since the IHD method for the regular(non-interface) cell is trivial, we mainly discuss the IHD formulation on interface cells and the related two and three dimensional VRTs. From here on we assume f is smooth throughout the domain for simplicity, then we can put $[\![f]\!] = 0$.

4.1 Hybrid difference method on the Q_2-grid cell

With reference to the cell configuration in Fig. 4 the cell finite difference is

$$-\varkappa^+ \Delta^h U^+(x_{22}) = -\varkappa^+ \frac{U^+_{32} - 2U^+_{22} + U^+_{12}}{(h_1/2)^2} - \varkappa^+ \frac{U^+_{23} - 2U^+_{22} + U^+_{21}}{(k_1/2)^2} = f(x_{22}) \tag{4.1}$$

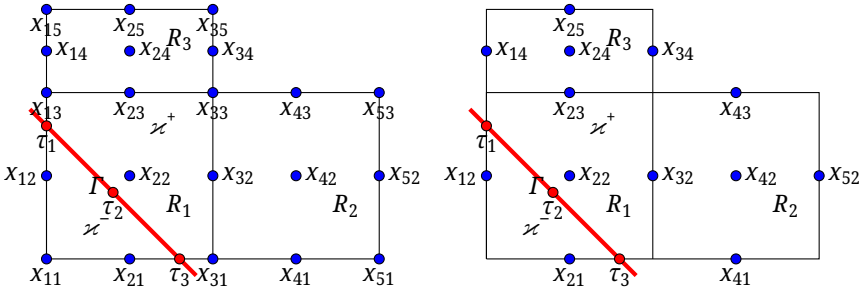

Fig. 4: The Q_2(left) and Q_2^*-grids: $|R_1| = h_1 \times k_1$, $|R_2| = h_2 \times k_1$, $|R_3| = h_1 \times k_2$.

on the cell R_1, and the intercell finite differences satisfy

$$[\![\partial_v^h U^+]\!]_x = \begin{cases} \frac{1}{h_1}(3U_{32}^+ - 4U_{22}^+ + U_{12}^+) + \frac{1}{h_2}(3U_{32}^+ - 4U_{42}^+ + U_{52}^+) = 0, & x = x_{32} \\ \frac{1}{k_1}(3U_{23}^+ - 4U_{22}^+ + U_{21}^+) + \frac{1}{k_2}(3U_{23}^+ - 4U_{24}^+ + U_{25}^+) = 0, & x = x_{23} \\ \frac{1}{h_1}(3U_{33}^+ - 4U_{23}^+ + U_{13}^+) + \frac{1}{h_2}(3U_{33}^+ - 4U_{43}^+ + U_{53}^+) = 0, & x = x_{33}. \end{cases} \tag{4.2}$$

Here,

$$U^{\text{real}} = [U_{11}^-, U_{21}^-, U_{31}^+, U_{12}^-, U_{22}^+, U_{32}^+, U_{13}^+, U_{23}^+, U_{33}^+]^T$$
$$U^{\text{virt}} = [U_{11}^+, U_{21}^+, U_{31}^-, U_{12}^+, U_{22}^-, U_{32}^-, U_{13}^-, U_{23}^-, U_{33}^-]^T.$$

In this case we will obtain the VRT as follows:

$$U^{\text{virt}} = \mathcal{M}U^{\text{real}} + \mathcal{L}[w(\tau_1), w(\tau_2), w(\tau_3), v(\tau_1), v(\tau_2), 0, 0, 0, 0]^T \tag{4.3}$$

by (4.4).

Remark 4.1.

- The intercell finite difference (4.2) is defined at all the other intercell points $\{x_{11}, x_{12}, x_{13}, x_{21}, x_{31}\}$ of R_1 as well if it is not a boundary point.
- According to [22] the intercell finite difference can be taken in either the x-axis direction or the y-axis direction at corner points. In (4.2) at x_{33} the x-axis parallel finite difference is used.

Then, the virtual values U^{virt} in (4.1) and (4.2) are replaced by the real values via the VRT (4.3). Moreover, the equation (4.3) is derived from the following equations. By Theorem 3.1 we have $\dim(\mathcal{N}_2) = 5$, therefore, the VRT should be composed of five interface conditions (three U-jumps and two flux jumps) as shown in equations (4.4a) and (4.4b). Again by Theorem 3.1 the system (4.4c) will be reduced to a linear system of rank four. Then, the total rank becomes nine, and the VRT is uniquely solvable. The Q_2-VRT is obtained by solving the following equations in an interface cell:

$$U^+(\tau_j) = U^-(\tau_j) + w(\tau_j), \qquad j = 1, 2, 3: \ U\text{-jump} \tag{4.4a}$$
$$\varkappa^+ \partial_{v^+} U^+(\tau_j) = -\varkappa^- \partial_{v^-} U^-(\tau_j) + v(\tau_j), \qquad j = 1, 2: \ \text{flux jump} \tag{4.4b}$$
$$-\varkappa^+ \Delta U^+(x_{kl}) = -\varkappa^- \Delta U^-(x_{kl}), \qquad k, l = 1, 2, 3: \ \text{consistency} \tag{4.4c}$$

for $U^\pm \in Q_2(x, y)$, which yields an overdetermined system, and it is solved by the QR factorization method.

4.2 Hybrid difference method on the Q_2^*-grid cell

With reference to the cell configuration in Fig. 4 the cell finite difference is

$$-\varkappa^+ \Delta^h U^+(x_{22}) = -\varkappa^+ \frac{U_{32}^+ - 2U_{22}^+ + U_{12}^+}{(h_1/2)^2} - \varkappa^+ \frac{U_{23}^+ - 2U_{22}^+ + U_{21}^+}{(k_1/2)^2} = f(x_{22}) \tag{4.5}$$

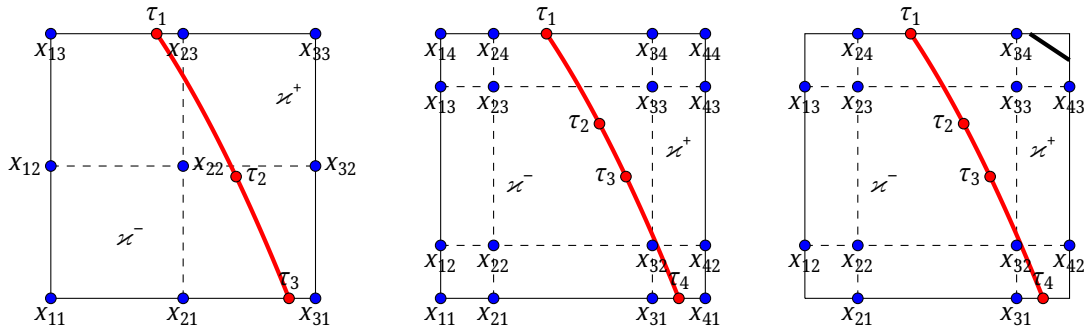

Fig. 5: The Q_2-grid (left), Q_3-grid cells (center), and Q_3^*-grid cells (right). The red solid curve represents a section of the interface. As the black line in the right plot, the interface that cut through an interface cell without dividing computational nodes is in the Q_m^* method.

on the cell R_1, and the intercell finite difference is

$$[\![\partial_\nu^h U^+]\!]_x = \begin{cases} \frac{1}{h_1}(3U_{32}^+ - 4U_{22}^+ + U_{12}^+) + \frac{1}{h_2}(3U_{32}^+ - 4U_{42}^+ + U_{52}^+) = 0, & x = x_{32} \\ \frac{1}{k_1}(3U_{23}^+ - 4U_{22}^+ + U_{21}^+) + \frac{1}{k_2}(3U_{23}^+ - 4U_{24}^+ + U_{25}^+) = 0, & x = x_{23}. \end{cases} \tag{4.6}$$

Remark 4.2.

– The intercell finite difference (4.6) is defined at all the (interior) intercell points x_{21} and x_{12} of R_1 as well.
– At corner points the intercell finite difference is not defined.

In the Q_2^* method we will obtain a smaller VRT and the total degrees of freedom for the global linear system is reduced as well. In three dimensional case we will have much more reduction in degrees of freedom both in the VRT and global stiffness system. We use $Q_2^*(x,y) = [1, x, y, x^2, y^2]$. Then, we need a VRT of rank five. In equations (4.7) it would be better to impose only two of the U-jump conditions in (4.7a), but we will keep it and solve the overdetermined system (4.7) for consistency of presentation with other higher order and higher dimensional methods. With reference to Fig. 4 we have

$$\begin{aligned} U^{\text{real}} &= [U_{21}^-, U_{12}^-, U_{22}^+, U_{32}^+, U_{23}^+]^T \\ U^{\text{virt}} &= [U_{21}^+, U_{12}^+, U_{22}^-, U_{32}^-, U_{23}^-]^T. \end{aligned}$$

In this case we will obtain the VRT as follows:

$$U^{\text{virt}} = \mathcal{M}U^{\text{real}} + \mathcal{L}[w(\tau_1), w(\tau_2), w(\tau_3), v(\tau_1), v(\tau_2)]^T.$$

Then, the virtual values U^{virt} in (4.5) and (4.6) are replaced by the real values via the VRT.

The Q_2^*-VRT is obtained from the following equations in an interface cell:

$$U^+(\tau_j) = U^-(\tau_j) + w(\tau_j), \qquad j = 1, 2, 3: \ U\text{-jump} \tag{4.7a}$$

$$\varkappa^+ \partial_{\nu^+} U^+(\tau_j) = -\varkappa^- \partial_{\nu^-} U^-(\tau_1) + v(\tau_j), \qquad j = 1, 2: \ \text{flux jump} \tag{4.7b}$$

$$-\varkappa^+ \Delta U^+(x_{kl}) = -\varkappa^- \Delta U^-(x_{kl}): \ \text{consistency} \tag{4.7c}$$

for $(k, l) = (2, 1), (1, 2), (2, 2), (3, 2), (2, 3)$ and $U^\pm \in Q_2^*(x,y) = [1, x, y, x^2, y^2]$.

Equations (4.4) and (4.7) are almost the same except the nodal points for the consistency condition.

4.3 Higher order VRTs on the Q_m and Q_m^*-cells

We mention again that the interior grids are the Gauss points in a cell.

For the Q_3-grid interface cell $\text{Rank}(\Delta Q_3(x,y)) = 8$ by Theorem 3.1. Therefore, we impose $8(= 16-8)$-interface conditions on four collocation points, that are composed of four U-jump and four flux-jump conditions. With

reference to Fig. 5 the Q_3-VRT is obtained by solving the overdetermined system

$$[\![U]\!]_p = w(p), \quad [\![\varkappa \partial_\nu U]\!]_p = v(p), \quad [\![-\varkappa \Delta U]\!]_{\mathbf{x}} = 0 \tag{4.8}$$

for $p \in \{\tau_1, \tau_2, \tau_3, \tau_4\} \subset \Gamma$, $\mathbf{x} = x_{ij}$ for $i, j = 1, 2, 3, 4$ and $U \in Q_3(x, y)$, and Q_3^*-VRT is obtained from

$$[\![U]\!]_p = w(p), \quad [\![\varkappa \partial_\nu U]\!]_p = v(p), \quad [\![-\varkappa \Delta U]\!]_{\mathbf{x}} = 0 \tag{4.9}$$

for $p \in \{\tau_1, \tau_2, \tau_3, \tau_4\} \subset \Gamma$, $\mathbf{x} \in Q_3^*$-grid, where Q_3^*-grid $= \{x_{ij} : i, j, = 1, 2, 3, 4\} \setminus \{x_{11}, x_{14}, x_{41}, x_{44}\}$ and $U \in Q_3^*(x, y) = P_3(x, y) \oplus [x^3 y, x y^3]$.

Since $Q_m(x, y)$ is a well-known polynomial space we pay our attention to $Q_m^*(x, y)$. Since $\deg(Q_m^*) = \deg(Q_m) - 4$, the $Q_m^*(m \geqslant 3)$-polynomial space is given as follows

$$Q_m^*(x, y) \equiv Q_m(x, y) \setminus [x^{m-1} y^{m-1}, x^m y^{m-1}, x^{m-1} y^m, x^m y^m] \tag{4.10}$$

so that it satisfies:

– $\deg(Q_m^*(x, y)) = \deg(Q_m(x, y)) - 4$;
– $\deg(\Delta Q_m^*(x, y)) + \deg(\mathcal{N}_m) \geqslant \deg(Q_m^*(x, y))$;
– $P_m(x, y) \subset Q_m^*(x, y)$ for $m \geqslant 3$.

By Theorem 3.1 we obtain the Q_m^*-VRT as follows:

$$[\![U]\!]_p = w(p), \quad [\![\varkappa \partial_\nu U]\!]_q = v(q), \quad [\![-\varkappa \Delta U]\!]_{\mathbf{x}} = 0 \tag{4.11}$$

for $\mathbf{x} = x_{ij}$ for $x_{ij} \in Q_m^*$-grid and $U \in Q_m^*(x, y)$. Here, $p, q \in \{\tau_1, \ldots, \tau_{m+1}\}$ when $m =$ odd, and $p \in \{\tau_1, \ldots, \tau_{m+1}\}$ and $q \in \{\tau_1, \ldots, \tau_m\}$ when $m =$ even.

4.4 Three dimensional VRTs on the Q_m^*-cell

Here, we only provide the Q_m^*-VRT and the $Q_m^*(x, y, z)$ polynomial space. By Theorem 3.2 the Q_m^*-VRT is obtained by solving the following overdetermined system:

$$[\![U]\!]_p = w(p), \quad [\![\varkappa \partial_\nu U]\!]_q = v(q), \quad [\![-\varkappa \Delta U]\!]_{\mathbf{x}} = 0 \tag{4.12}$$

for $\mathbf{x} \in Q_m^*$-grid and $U \in Q_m^*(x, y, z)$. Here, $\#(p) = \#(q)$ when $m =$ odd, and $\#(p) = \#(q) + 1$ when $m =$ even, while $\#(p) + \#(q) = \dim(\mathcal{N}_m)$.

To define three dimensional VRT on the Q_m^*-cell the following properties are required to be satisfied by $Q_m^*(x, y, z)$:

– $\deg(Q_m^*(x, y, z)) = \deg(Q_m(x, y, z)) - 12m + 4$;
– $\deg(\Delta Q_m^*(x, y, z)) + \deg(\mathcal{N}_m) \geqslant \deg(Q_m^*(x, y, z))$;
– $P_m(x, y, z) \subset Q_m^*(x, y, z)$ for $m \geqslant 3$.

We provide a systematic way of choosing $Q_m^*(x, y, z)$ as follows:

$$Q_m^*(x, y, z) = \operatorname{span}\{x^i y^j z^k \mid i, j, k = 0, \ldots, m, \ \max\big(\min(i, j), \min(j, k), \min(i, k)\big) < m - 1\}.$$

For an example,

$$Q_3^*(x, y, z) = P_3(x, y, z) \oplus [x^3 y, x y^3, y^3 z, y z^3, z^3 x, z x^3, x^2 y z, x y^2 z, x y z^2, x^3 y z, x y^3 z, x y z^3].$$

Remark 4.3. In the right plot of Fig. 5 the black cut is ignored in the Q_m^* method, but it will not be ignored in the Q_m method. As its length becomes smaller the Q_m-VRT can be more ill-conditioned since the interface conditions are imposed on a small section of an interface, and it eventually becomes singular if this intersection becomes one point. Therefore, we prefer to use the Q_m^* method to avoid possible occurrence of instability. Moreover, the Q_m^* method yields a much smaller linear system in the 3D case.

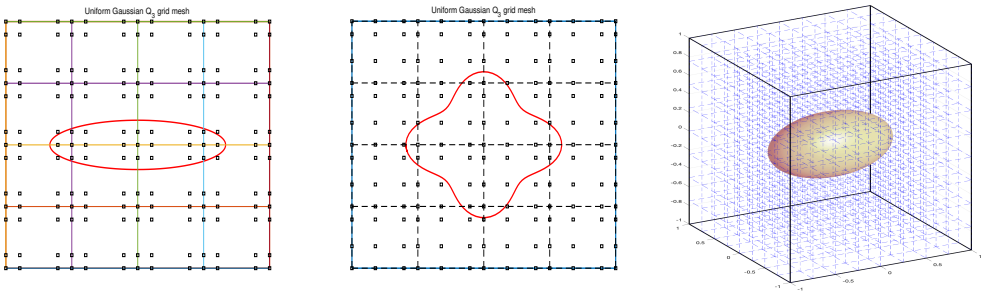

Fig. 6: The ellipse, four-leafed flower and ellipsoid.

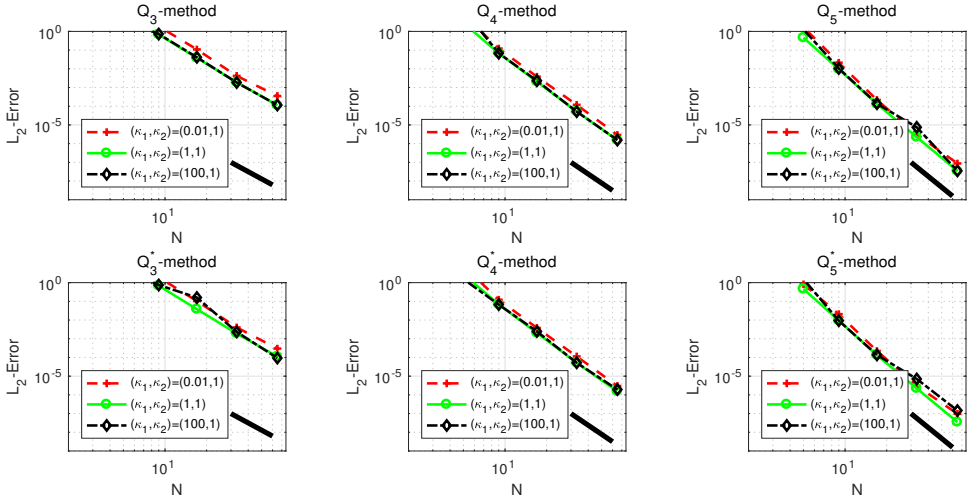

Fig. 7: The L_2 error and convergence rate for the Q_m(top) and Q_m^*(bottom) methods for Example 5.1. Here, $(\varkappa_1, \varkappa_2) = (\varkappa^-, \varkappa^+)$. The bold black line segment represents the theoretically expected rate of convergence with slope $m + 1$.

5 Numerical experiments

We provide two and three dimensional numerical examples with the three interfaces as in Fig. 6. Numerical experiments were performed on the Q_m and Q_m^* grids with $m = 3, 4, 5$. Errors are measured in the discrete L_2 and H^1-norms.

In the IHD one wish to use a fixed mesh (especially, a uniform mesh), independently of the shape of an interface. Then, it is inevitable to have some segments of interface ignored in the Q_m^* method. An interface cell is called a *coherent* interface cell if the interface divides computational nodes into two nonempty sets. If there are too many non-coherent interface cells it can cause some poor convergence in numerical solution. According to our numerical experiments the ratio, for a broad class of interfaces,

$$\text{coherence ratio} = \frac{\#(\text{coherent interface cells})}{\#(\text{total interface cells})}$$

is high enough to guarantee the optimal order of convergence of numerical solutions if $m \geqslant 3$. For a detailed discussion see [9].

Example 5.1. An elliptic equation on the domain with an elliptic interface $\Gamma = \{(x, y) : k(x, y) = 1\}$, $k(x, y) = \frac{9}{4}x^2 + 25y^2$ is solved on the uniform Q_m and Q_m^* mesh grids with $m = 3, 4, 5$. The exact solution is given as

$$u(x, y) = \begin{cases} \sin(k(x, y) - 1)/\varkappa^- + x + y, & k(x, y) < 1 \\ \sin(k(x, y) - 1)/\varkappa^+, & k(x, y) \geqslant 1 \end{cases}$$

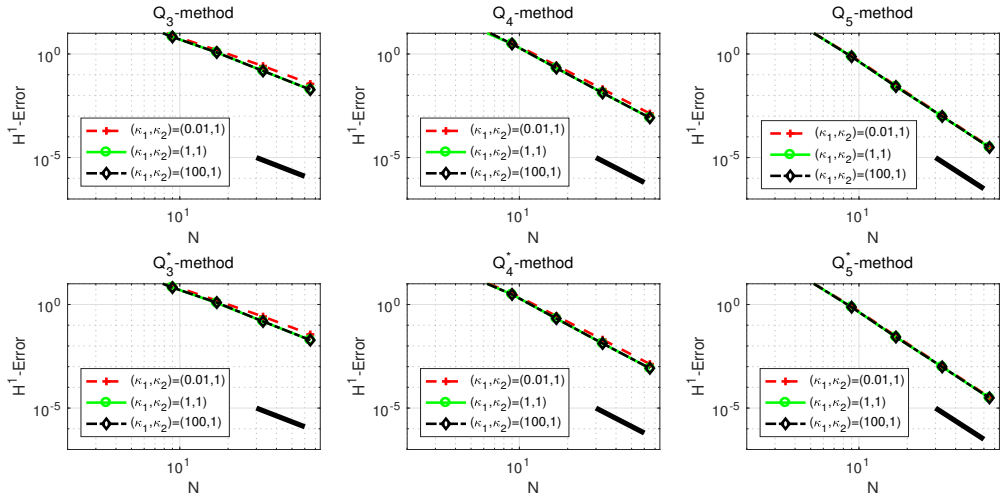

Fig. 8: The H^1-norm error and convergence rate for the Q_m(top) and Q_m^*(bottom) methods for Example 5.1. The bold black line segment represents the theoretically expected rate of convergence with slope m.

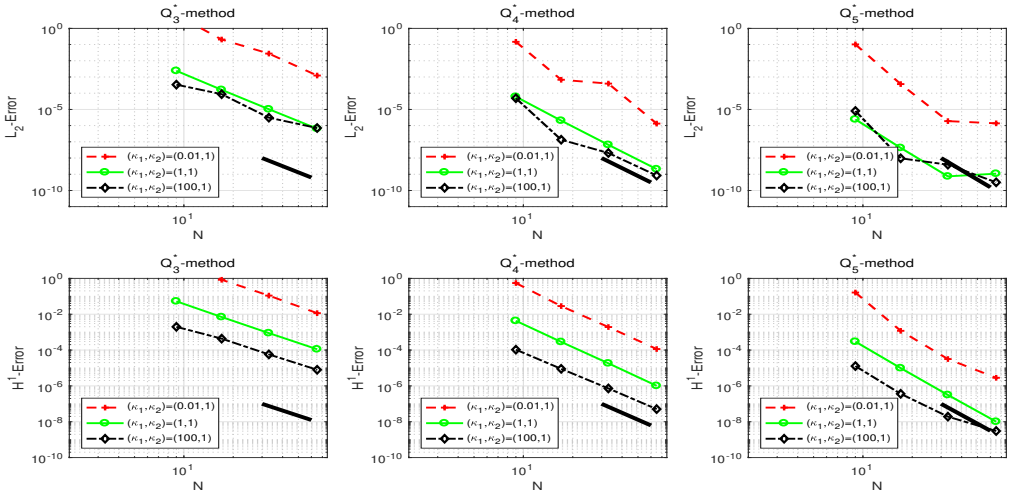

Fig. 9: The L_2 and H^1-norm errors and convergence rates for the Q_m^* methods for Example 5.2. The bold black line segment represents the rate of the theoretically expected convergence with slopes $m+1$ and m for the L_2 and H^1-errors, respectively.

with $(\varkappa^-, \varkappa^+) = (0.01, 1),\ (1, 1),\ (100, 1)$. The solution satisfies the elliptic equation

$$-\nabla\cdot(\varkappa\nabla u) = f \qquad \text{on } [-1,1]\times[-1,1]$$

with a smooth f (therefore, $[\![f]\!] = 0$) and the interface conditions,

$$[\![u]\!]_\Gamma = -(x+y), \qquad [\![\varkappa\partial_\nu u]\!]_\Gamma = \varkappa^-(\nu_1+\nu_2)$$

where $\nu = (\nu_1, \nu_2)$ are the outward unit normal vector on Γ from Ω^-. Figures 7, 8, and 10 represent numerical results for Example 5.1.

In Example 5.1 the interface is an ellipse and both the Q_m and Q_m^* methods are tested. As shown in Figs. 7 and 8 convergence orders concord very well with the theoretically expected ones, $O(h^{m+1})$ and $O(h^m)$ in the L_2 and H^1-norms, respectively. We can not find any difference in convergence and numerics between the Q_m and Q_m^* methods. As shown in Fig. 10 the error is concentrated around the domain boundary rather than the interface.

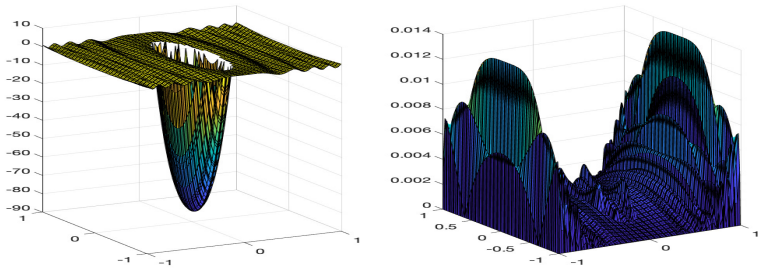

Fig. 10: The solution and error distribution for Example 5.1. Here, $(\varkappa^-, \varkappa^+) = (0.01, 1)$ and computation is performed with the Q_4^* method and $N = 32$.

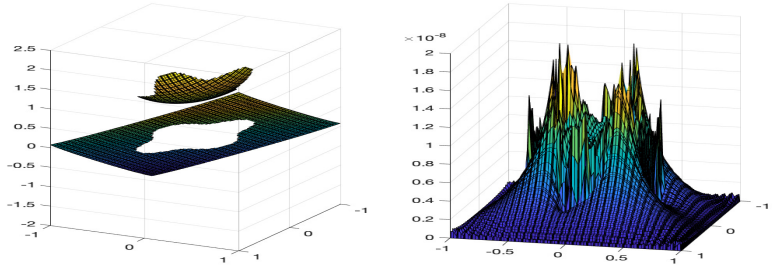

Fig. 11: The solution and error distribution for Example 5.2. Here, $(\varkappa^-, \varkappa^+) = (100, 1)$ and computation is performed with the Q_4^* method and $N = 32$.

Example 5.2. The elliptic interface problem is solved on the domain with the interface; $r = \frac{1}{2} + \frac{1}{11}\cos(4\vartheta)$ in the polar coordinate system. The exact solution is given as

$$u(x,y) = \begin{cases} \exp(x^2+y^2)/\varkappa^- + \exp(x)\cos(y), & r < \frac{1}{2} + \frac{1}{11}\cos(4\vartheta) \\ \exp(x^2+y^2)/\varkappa^+, & \text{otherwise.} \end{cases}$$

Hence, $[\![f]\!] = 0$, and the solution satisfies the interface conditions,

$$[\![u]\!]_\Gamma = \exp(x^2+y^2)\left(\frac{1}{\varkappa^+} - \frac{1}{\varkappa^-}\right) - \exp(x)\cos(y), \qquad [\![\varkappa\partial_\nu u]\!]_\Gamma = \varkappa^- \exp(x)(\nu_1\cos(y) - \nu_2\sin(y)).$$

For this problem only the Q_m^* $(m = 3, 4, 5)$ method is tested with $(\varkappa^-, \varkappa^+) = (0.01, 1),\ (1, 1),\ (100, 1)$. Figures 9 and 11 represent numerical results for Example 5.2.

In Example 5.2 the interface is non-convex and of more complicated geometric shape than an ellipse. For this we perform numerical experiments only with the Q_m^* method. The geometry of interface seems to have influence on convergence in the sense that convergence is less regular than that of Example 5.1. The H^1-norm convergence is more regular than that of the L_2-norm, which is commonly observed in finite difference methods. The errors are much less since the test function is much regular than that of Example 5.1. In this case error is more distributed around the interface as shown in Fig. 11.

Example 5.3. Consider three dimensional interface problem. The ellipsoidal interface satisfies $\frac{x^2}{a^2} + \frac{y^2}{b^2} + \frac{z^2}{c^2} = 1$ with $a = 16/23,\ b = c = 8/23$. The exact solution is given as

$$u(x,y,z) = \begin{cases} \exp(x+y+z)/\varkappa^- + (x^2+y^2+z^2)/\varkappa^-, & \frac{x^2}{a^2} + \frac{y^2}{b^2} + \frac{z^2}{c^2} < 1 \\ \exp(x+y+z)/\varkappa^+, & \text{otherwise.} \end{cases}$$

Then, it satisfies $[\![f]\!] = 6$ and the interface conditions,

$$[\![u]\!]_\Gamma = \exp(x+y+z)\left(\frac{1}{\varkappa^+} - \frac{1}{\varkappa^-}\right) - \frac{x^2+y^2+z^2}{\varkappa^-}, \qquad [\![\varkappa\partial_\nu u]\!]_\Gamma = 2(x\nu_1 + y\nu_2 + z\nu_3).$$

Tab. 1: Convergence history of the Q_3^* method for Example 5.3.

	(0.1, 1)				(10, 1)			
N	L_2	rate	H^1	rate	L_2	rate	H^1	rate
4	6.0273e-03	—	2.3046e-02	—	5.4947e-02	—	1.0448e-01	—
8	1.6511e-03	1.87	8.0410e-03	1.52	5.1551e-03	3.41	1.3469e-02	2.96
10	6.7181e-04	4.03	5.1157e-03	2.03	1.6795e-03	5.03	4.7311e-03	4.69
14	1.5021e-04	4.45	1.0410e-03	4.73	9.2579e-05	8.61	6.7791e-04	5.77
16	7.2805e-05	5.42	6.0831e-04	4.02	2.9291e-05	8.62	3.9419e-04	4.06

Tab. 2: Comparison of the degrees of freedom for the 3D case. The number 20/27 represents an asymptotic ratio for a big N.

	VRT	Total
Q_m	$(m+1)^3$	$(mN+1)^3$
Q_m^*	$(m+1)^3 - 12m + 4$	$(mN-N)^2(mN+2N+3)$
Q_3^*/Q_3	1/2	20/27

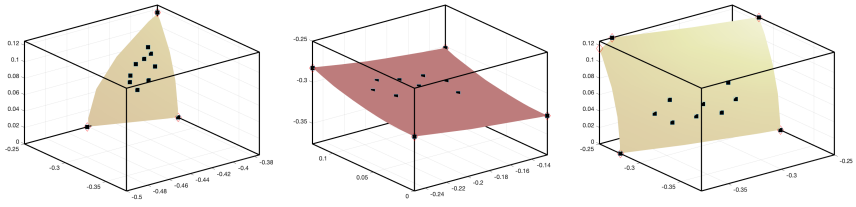

(a) 3-ints. pts. **(b)** 4-ints. pts. **(c)** 5-ints. pts.

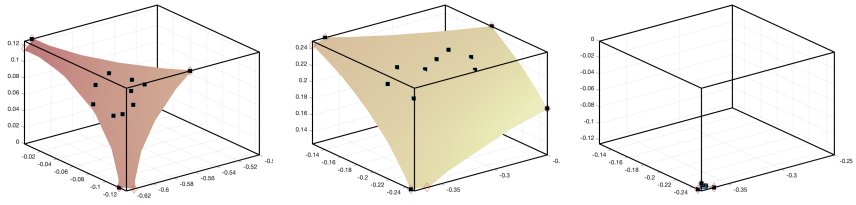

(d) 5-ints. pts. **(e)** 6-ints. pts. **(f)** non-coherent

Fig. 12: Common cell-wise patterns of the ellipsoidal interface. The digit in the subcaption is the number of intersections with cell edges. The black markers represent the 12-collocation points where the interface conditions are applied.

Only the Q_3^* method is tested with $(\varkappa^-, \varkappa^+) = (0.1, 1),\ (10, 1)$.

For Example 5.3 we consider only the Q_3^* method on an ellipsoid. The test function is chosen to have non-homogeneous jump in the consistency condition. As shown in Table 1, because of heavy computational cost numerical experiment is performed only for up to $h = 1/8$, therefore, we could not observe a saturated order of convergence. However, we expect a theoretically expected convergence when the number of subdivision is increased. Table 2 shows that the Q_m^* method has much less degrees of freedom than the Q_m method for three dimensional problems. In the case of the Q_3^* method the degrees of freedom in the VRT become a half and the global system size is reduced by almost a quarter. Therefore, it is strongly recommended to use the Q_m^* method as a stable and effective numerical solver for three dimensional problems. Figures 12 shows some major cell-wise patterns of the ellipsoidal interface. Non-coherent interface cell (the bottom right in Fig. 12) seems to happen more frequently as the mesh becomes finer, in which case clustering of collocation points can be a source of instability in the VRT for the Q_m method.

6 Conclusion

The immersed hybrid difference method with high order convergence for two and three dimensional elliptic interface problems is introduced and related numerical experiments are performed. The key contributions of the paper are (1) finding the exact number of collocation points for interface conditions (2) finding a unique way of constructing the Q_m^*-polynomial space. The Q_m^* and Q_m methods with $m \geqslant 3$ have almost the same convergence property, while the Q_m^* method contains much less degrees of freedom (especially in three dimension) and it looks more reliable for interfaces of complicated geometric shapes. A less desirable feature of the IHD method, compared to the MIB method, is that the VRT becomes of a large size especially for three dimensional problems with high order methods. However, the VRT is independent from a cell to a cell, hence this process can be parallelized by nature.

Funding: This author was supported by NRF 2022R1F1A107272211.

References

[1] S. Adjerid, I. Babuška, R. Guo, and T. Lin, An enriched immersed finite element method for interface problems with nonhomogeneous jump conditions, *Computer Methods in Applied Mechanics and Engineering* **404** (2023), 1–37.

[2] J. Chessa, P. Smolinski, and T. Belytschko, The extended finite element method(XFEM) for solidification problems, *Int. J. Numer. Methods Engrg.* **53** (2002), 1959–1977.

[3] Q. Feng, B. Han, and P. Minev, Sixth order compact finite difference schemes for Poisson interface problems with singular sources, *Comp. Math. Appl.* **99** (2021), 2–25.

[4] Q. Feng, B. Han, and P. Minev, A high order compact finite difference scheme for elliptic interface problems with discontinuous and high-contrast coefficients, *Appl. Math. Comp.* **431** (2022), 1–24.

[5] R. Guo and T. Lin, A higher degree immersed finite element method based on a Cauchy extension for elliptic interface problems, *SINUM* **57** (2019), 1545–1573.

[6] X.-M. He, T. Lin, and Y. Lin, A bilinear immersed finite volume element method for the diffusion equation with discontinuous coefficient, *Comm. in Comp. Phys.* **6** (2009), No. 1, 185–202.

[7] H. Huang and Z. Li, Convergence analysis of the immersed interface method, *IMA J. Numer. Anal.* **19** (1999), No. 4, 583–608.

[8] Y. Jeon, Hybrid difference methods for PDEs, *J. Sci. Comput.* **64** (2015), 508–521.

[9] Y. Jeon, An immersed hybrid difference method for the elliptic interface equation, *Japan J. Industr. App. Math.* **39** (2022), 669–692.

[10] Y. Jeon, E.-J. Park, and D.-W. Shin, Hybrid spectral difference methods for an elliptic equation, *Comput. Meth. Appl. Math.* **17** (2017), 253–267.

[11] Y. Jeon and D. Sheen, Upwind hybrid spectral difference methods for the steady–state Navier–Stokes equations, In: *Contemporary Computational Mathematics — A Celebration of the 80th Birthday of Ian Sloan* (Eds. J. Dick and F. Y. Kuo), Springer-Verlag, 2018, pp. 632–641.

[12] Y. Jeon and S.-Y. Yi, The immersed interface hybridized difference method for parabolic interface problems, *Numer. Math. Theor. Meth. Appl.* **15** (2022), 336–359.

[13] M. C. Lai and C. S. Peskin, An immersed boundary method with formal second-order accuracy and reduced numerical viscosity, *J. Comput. Phys.* **160** (2000), 705–719.

[14] R. J. LeVeque and Z. Li, The immersed interface method for elliptic equations with discontinuous coefficients and singular sources, *SIAM J. Numer. Anal.* **31** (1994), No. 4, 1019–1044.

[15] R. J. LeVeque and Z. Li, Immersed interface methods for Stokes flow with elastic boundaries or surface tension, *SIAM J. Sci. Comput.* **18** (1997), No. 3, 709–735.

[16] Z. Li and K. Ito, *The Immersed Interface Method: Numerical Solutions of PDEs Involving Interfaces and Irregular Domains, Frontiers in Applied Mathematics*, SIAM Pub., 2006.

[17] Z. Li, T. Lin, Y. Lin, and R. C. Rogers, An immersed finite element space and its approximation capability, *Numer. Meth. PDEs* **20** (2004), No. 3, 338–367.

[18] A. N. Marques, J.-C. Nave, and R. R. Rosales, High order solution of Poisson problems with piecewise constant coefficients and interface jumps, *J. Comp. Phys.* **335** (2017), 497–515.

[19] A. N. Marques, J.-C. Nave, and R. R. Rosales, A correction function method for Poisson problems with interface jump conditions, *J. Comp. Phys.* **230** (2011), 7567–7597.

[20] R. Mittal and G. Iaccarino, Immersed boundary methods, *Annu. Rev. Fluid Mech.* **37** (2005), 239–261.

[21] C. S. Peskin, The immersed boundary method, *Acta Numer.* **11** (2002), 479–517.

[22] D. Shin, Y. Jeon, and E.-J. Park, A novel hybrid difference method for an elliptic equation, *Applied Mathematics and Computation* **415** (2022).
[23] W. Ying and C. Henriquez, A kernel-free boundary integral method for elliptic boundary value problems, *J. Comput. Phys.* **227** (2007), 1046–1074.
[24] W. Ying and W.-C. Wang, A kernel-free boundary integral method for variable coefficient elliptic pdes, *Comm. Comput. Phys.* **15** (2014), 1108–1140.
[25] Y. C. Zhou, M. FeigS. Zhao, and G. W. Wei, High order matched interface and boundary method for elliptic equations with discontinuous coefficients and singular sources, *J. Comput. Phys.* **213** (2006), 1–30.
[26] Y. C. Zhou and G. W. Wei, On the fictitious-domain and interpolation formulations of the matched interface and boundary (MIB) method, *J. Comput. Phys.* **219** (2006), 228–246.